PAPER

Check for updates

Hypercrosslinked polymers for oil adsorption: the influence of porosity and fluorine incorporation

Le Tang, [a] Paul Schweng, [a,b] Joseph J. Dale [a] and Robert T. Woodward [*a]

The selective removal of oil and oil-based contaminants from water remains a critical challenge in environmental remediation. Here, we report a series of hypercrosslinked polymers with high surface areas and tuneable chemistries, achieving exceptional adsorption capacities for a variety of organic solvents, with a maximum capacity of >15 g g^{-1} for chlorinated solvents. We describe how the adsorption capacities of the materials in pure organic solvents are governed by porosity rather than sample fluorine content and its associated hydrophobicity, challenging conventional design strategies. Oil/water separation tests of the most promising networks demonstrated the effective removal of toluene from water, achieving separation efficiencies of >99%. The polymers also exhibit exceptional stability in organic solvents, allowing repeated use. This work establishes hypercrosslinked polymers as robust, scalable materials for efficient oil−water separation and advanced wastewater treatment.

Introduction

The remediation of oil pollution in aquatic environments presents broad technical and environmental challenges, owing to the complexity and scale of contamination events.[1] Marine transport, offshore drilling, and land-based runoffs collectively account for vast quantities of oil entering water bodies each year. Since 1970, an estimated 10 million tonnes of oil have been spilt into aquatic systems, including the release of around 4.9 million barrels of crude oil during the 2010 Deepwater Horizon incident.[2] The hydrophobic nature and low water solubility of oil-based contaminants mean they typically accumulate as a separate bulk phase, forming slicks or emulsions that are difficult to treat. Upon release, these hydrocarbons can spread over large surface areas, smothering coastlines, or spreading for hundreds of miles across bodies of water in a thin oil slick and disrupting delicate aquatic ecosystems.[3] Beyond ecological damage, oil spills also pose serious socioeconomic challenges and, as such, urgently require efforts toward more effective mitigation strategies.

Current oil remediation technologies face numerous limitations, particularly in separating immiscible oil from water. Skimmers and dispersants are commonly used, yet are energy-intensive, limited in effectiveness, and often cause secondary pollution.[1] Adsorbent materials capable of selectively capturing large amounts of bulk-phase oils have garnered attention as attractive alternatives. Ideal sorbents should exhibit high uptake capacity, hydrophobicity, rapid adsorption, structural durability, and reusability. Achieving all these features simultaneously, while ensuring scalability and economic viability, remains a major challenge for adsorbent material design. Efforts have focused on developing various hydrophobic porous frameworks, including sponges,[4,5] membranes,[6,7] fabrics,[8,9] and aerogels,[10] However, many such systems are hampered by complicated synthesis routes, lack of durability, or challenging regeneration procedures.

Hypercrosslinked polymers (HCPs) may represent a promising alternative platform for oil sorption and water remediation. These amorphous polymer networks possess high surface areas, tuneable pore structures, swellability, and exceptional chemical stability, and can be synthesised from inexpensive, commercially available monomers.[11–13] HCPs have shown excellent performance in both gas phase adsorption, such as atmospheric water harvesting,[14,15] CO$_2$ capture,[16] and the capture of volatile organic compounds,[17,18] as well as in the adsorption of dissolved pollutants.[19,20] However, their potential for bulk-phase organic solvent uptake and direct oil/water separation remains relatively underexplored. Superhydrophobic monolithic adsorbents used for oil/water emulsion separation and oil recovery have been produced via the coating or anchoring of HCPs onto melamine formaldehyde sponges.[5,21,22] The coated sponges showed ultrahigh separation efficiency and outstanding durability. Elsewhere, Lin et al. fabricated hypercrosslinked microporous polymers via emulsion-templating, demonstrating that the incorporation of fluorine substantially enhanced both hydrophobicity and oil adsorption capacity.[23]

*a*Institute of Materials Chemistry and Research, Faculty of Chemistry, University of Vienna, Währinger Straße 42, 1090 Vienna, Austria.
E-mail: robert.woodward@univie.ac.at
*b*Vienna Doctoral School in Chemistry, University of Vienna, Währinger Straße 42, 1090 Vienna, Austria

Powdered or particulate adsorbents are particularly efficient in cleaning high viscosity or large-area thin oil spills when compared with monolithic adsorbents, however, the oil adsorption capacities of powders remain limited in comparison[24] A powdered superhydrophobic covalent organic framework showed a crude oil uptake capacity of almost 12 g g^{-1} after post-functional hydrophobisation *via* silane grafting.[25] Activated carbons have also shown promise for oil sorption, with lauric acid decorated biochar achieving an oil uptake capacity of 11 g g^{-1} (ref. 26) and magnetite-loaded carbons offering facile separation using magnetic fields.[27] However, further work is needed in order to improve uptake capacities and unveil simpler routes to effective adsorbents.

In this work, we synthesise both non-functional and fluorine-containing HCPs by the simple self-polycondensation of 4,4′-bis(chloromethyl)biphenyl (BCMBP) and α,α′-dichloro-*p*-xylene (*p*DCX).[28] To investigate the impact of chemical composition on adsorption and separation performance, the fluorine-containing monomer 4-fluorobenzyl chloride (*p*FBC) is incorporated into the HCP structure in varying ratios. Given the hydrophobic nature of fluorine, its incorporation was expected to enhance oil adsorption and improve oil/water separation. The resulting materials are evaluated for their chemical composition, porosity, organic solvent uptake, and separation efficiency, offering insights into structure–property relationships in these HCP-based adsorbents.

Experimental

Materials

4,4′-Bis(chloromethyl)biphenyl (BCMBP, 95%), α,α′-dichloro-*p*-xylene (*p*DCX, 98%), FeCl$_3$ (97%), Sudan III (≥85%), 1,2-dichloroethane (DCE, ≥99.0%), methanol (≥99.8%), toluene (≥99.7%), and *n*-heptane (≥99%) were purchased from Sigma-Aldrich. 4-Fluorobenzyl chloride (*p*FBC, >98%) and benzotrifluoride (BTF, >98%) were purchased from Tokyo Chemical Industry. All chemicals were used as received.

Hypercrosslinked polymer synthesis

Monomer(s) (details shown in Table 1) and DCE (30 mL) were added to a 100 mL two-neck round bottom flask and stirred at ~100 rpm. After monomer dissolution, FeCl$_3$ (0.73 g, 4.5 mmol, 1.5 eq.) was added and the mixture was refluxed at 80 °C for 14 h. After cooling to room temperature, the resulting solid was filtered with a Büchner funnel, washed with 100 mL of methanol on the filter, and then by Soxhlet extraction with methanol for a further 22 h. The washed HCPs were placed in a fume cupboard overnight to allow excess solvent to evaporate, ground into a fine powder using a pestle and mortar, and dried in a vacuum oven at 80 °C overnight, yielding brown/dark brown powders. Networks derived from BCMBP and *p*DCX are named BP-HCP(-XF) and X-HCP(-XF), respectively, where XF represents the theoretical mol% of *p*FBC, if present.

Characterisation

Fourier-transform infrared (FTIR) spectra were collected with a Tensor II FTIR spectrometer (Bruker) equipped with a Bruker Platinum-ATR Convenience sampling module at room temperature. Each spectrum was measured with 32 scans in the range of 400 to 4000 cm^{-1} with a resolution of 4 cm^{-1} and was recorded and analysed using the OPUS 7.5 software.

Thermogravimetric analysis (TGA) was conducted using a Discovery TGA (TA instruments). Between 3 to 10 mg of sample was placed into a platinum sample pan, equilibrated at 30 °C, then heated to 800 °C at a ramp rate of 10 °C min^{-1} in air. Samples were held at the target temperature for 5 min before being allowed to cool. The TGA data were recorded and analysed using the Discovery TGA@Lab program in TRIOS software.

X-ray photoelectron spectroscopy (XPS) was performed on a Nexsa Photoelectron Spectrometer (Thermo Scientific). All measurements were performed using Al-Kα X-rays with a spot size of 400 μm. The survey spectra were taken at a pass energy of 200 eV from 1350 to 0 eV with a resolution of 1 eV. The high-resolution C 1s, O 1s, F 1s, and Cl 2p spectra were collected at a pass energy of 50 eV with a resolution of 0.1 eV. C 1s was collected in the range from 298 to 279 eV, O 1s from 545 to 525 eV, F 1s from 698 to 678 eV, and Cl 2p from 210 to 190 eV.

The N$_2$ adsorption–desorption isotherms were measured at −196 °C using a 3Flex (Micromeritics), or a TriStar II (Micromeritics) for sample repeats. Before the measurement, 50 to 100 mg of sample was degassed at 120 °C under N$_2$ flow for 14 h using a FlowPrep 060 (Micromeritics). The networks' specific surface areas (SSA) were determined *via* the Brunauer–Emmett–Teller (BET) method in the relative pressure P/P_0 range 0.05 to 0.3. Pore size distributions (PSDs) were determined from the N$_2$ adsorption branch of the isotherm using quenched solid density functional theory (QSDFT) and a carbon model with slit/cylindrical pores. The total pore volume V_P, micropore volume V_{Mic}, and mesopore volume V_{Mes} were determined from the cumulative pore volumes calculated using QSDFT in the relevant pore width ranges. When calculating V_P and V_{Mes}, isotherm points from $P/P_0 > 0.97$ were excluded to avoid the effects of bulk N$_2$ condensation.

Dynamic vapour sorption (DVS) experiments were performed on a DVS-Discovery (Surface Measurement Systems). Approximately 10 mg of sample was weighed into a quartz crystal pan. Each experiment was performed at 25 °C and either deionised water (HPLC grade) or toluene (HPLC grade) was used to generate the desired relative pressure. Each ana-

Table 1 Monomeric composition of all synthesised HCPs

Network	Monomer feedstock composition			
	Monomer 1	*n* (mmol)	Monomer 2	*n* (mmol)
BP-HCP	BCMBP	3	—	—
BP-HCP-25F	BCMBP	3	*p*FBC	1
BP-HCP-50F	BCMBP	3	*p*FBC	3
X-HCP	*p*DCX	3	—	—
X-HCP-25F	*p*DCX	3	*p*FBC	1
X-HCP-50F	*p*DCX	3	*p*FBC	3

lysis commenced at a relative pressure of 0.0 P/P_0 and was increased to the desired P/P_0 for sorbate uptake. Isotherms were recorded up to 0.9 P/P_0, using a step increment of 0.1. Each step was equilibrated until the weight change was below 0.005% min^{-1} prior to data point collection.

Oil adsorption

To determine oil adsorption capacity, approximately 45 mg of HCP was suspended in solvent (10 mL) in a covered glass vial and stirred at 250 rpm for 1 h. After stirring, HCPs were vacuum filtered in a Büchner funnel to remove excess solvent, removed from the filter paper, and quickly reweighed to minimise solvent evaporation. The mass of the recovered adsorbents after drying was typically 35–45 mg, indicating a mass loss in filtration of up to 10 mg. The networks were then dried at 120 °C for at least 16 h and reweighed. Each measurement was repeated 5 times to ensure reproducibility, and adsorption capacity k_D was calculated using eqn (1):

$$k_D = \frac{m_A - m_D}{m_D} \qquad (1)$$

where m_A and m_D are the weight of the sample after adsorption and after drying, respectively.

For comparison, the adsorption capacity k_B based on the dry weight of the sample before adsorption was calculated according to eqn (2), following previous reports:[5,22,23,27]

$$k_B = \frac{m_A - m_B}{m_B} \qquad (2)$$

where m_B is the weight of the sample before adsorption.

Oil/water separation experiments

To demonstrate the separation of immiscible organic solvent from water, toluene and distilled water were selected as organic and aqueous phases, respectively. To visualise the separation, toluene was dyed using fat-soluble dye Sudan III (0.01 g mL^{-1}). The oil/water mixture was prepared in a 25 mL graduated cylinder using 0.5 mL of Sudan III dyed toluene and 20 mL of distilled water, followed by the addition of samples in portions while shaking gently until no red organic phase could be observed. The samples considered in this test were BP-HCP (88.1 mg) and BP-HCP-25F (87.0 mg). After adsorption, samples were removed by vacuum filtration and the oil/water separation efficiency SE was calculated using eqn (3), as reported by Sarkar et al.:[29]

$$SE = \frac{m_{Wr}}{m_{Wi}} \times 100\% \qquad (3)$$

where m_{Wi} and m_{Wr} were the initial weight of water and the weight of the remaining water after separation, respectively. The adsorption efficiency AE of samples during oil/water separation was calculated using eqn (4):

$$AE = \frac{m_{St}}{m_{Sa}} \times 100\% \qquad (4)$$

where m_{St} and m_{Sa} were the theoretical (based on their isolated adsorption capacities) and actual masses of the HCPs used in the separation experiment, respectively. Additionally, 20 mL of water alone was used as a control to measure any potential loss during vacuum filtration.

Results and discussion

Synthesis and characterisation of HCPs

Six HCPs were synthesised using either BCMBP or pDCX as a framework monomer/crosslinker and pFBC as a fluorine-containing monomer (Fig. 1a and b). All networks were synthesised via an FeCl$_3$ catalysed Friedel–Crafts alkylation in 1,2-dichloroethane. Further synthesis details are provided in the Experimental section. The resulting polymers were named according to their monomeric composition, as detailed in Table 1. Networks derived from BCMBP, which contain a biphenyl-based skeleton, are designated BP-HCP(-XF), where X represents the theoretical mol% of pFBC. For networks synthesised from pDCX, the notation X-HCP(-XF) is used. All HCPs were brown powders produced in yields of >86%. We also attempted the self-polycondensation of pFBC alone, however poor yields prevented us from pursuing this polymer further.

The FTIR spectra of BP-HCPs (Fig. 1c) displayed the characteristic absorption peaks of the 4,4′-dimethylbiphenyl framework, with BP-HCP-25F and BP-HCP-50F exhibiting three additional peaks at 1228, 1157 and 501 cm^{-1}. The peaks at 1228 and 1157 cm^{-1} were assigned to C–H in-plane bending vibration in the fluorinated aromatic ring, and the peak at 501 cm^{-1} was assigned to the characteristic C$_{Ar}$–F bending vibration, confirming the incorporation of fluorine. The C$_{Ar}$–F stretching vibration expected at around 1330 cm^{-1} was likely overlapped by other signals and was not observed. Increasing pFBC content led to a greater intensity of peaks associated with fluorine, indicative of BP-HCP-50F containing the highest fluorine content of the BP-HCPs. A similar trend was observed in the X-HCP series (Fig. 1d), where X-HCP-25F and X-HCP-50F exhibited the same three additional peaks at 1233, 1157 and 501 cm^{-1}, relative to X-HCP, confirming successful pFBC incorporation. Again, peaks associated with fluorine increased with expected pFBC content, indicating X-HCP-50F contained the highest fluorine content of the X-HCPs. The FTIR spectra of the BP-HCPs after 6 months storage in ambient conditions were almost the same as their corresponding pristine spectra (Fig. S1), confirming the excellent stability of HCPs.

XPS was conducted to understand the surface chemistry and relative fluorine content of all HCPs. Survey spectra (Fig. 1e and f) confirmed the presence of fluorine in all networks produced from monomer feeds containing pFBC, as well as the presence of residual terminal chlorine. The pFBC was incorporated effectively with increasing pFBC monomer ratios, with BP-HCP-50F and X-HCP-50F reaching fluorine contents of 6.0 ± 0.4 at% and 7.1 ± 0.1 at%, respectively. The fluorine content of all networks was in slight excess of the theore-
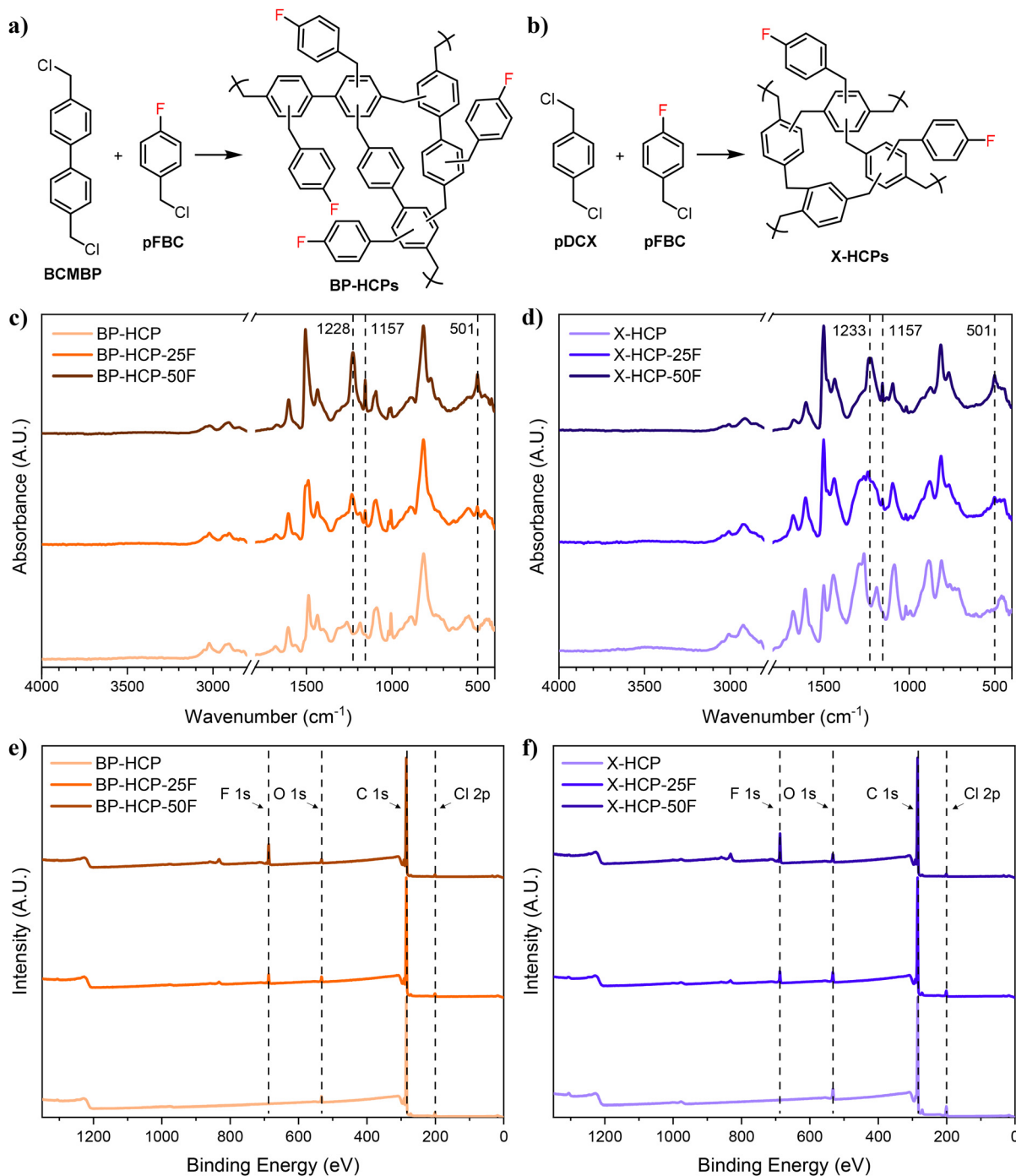
Fig. 1 (a) Reaction scheme for the synthesis of BP-HCPs, (b) reaction scheme for the synthesis of X-HCPs, (c) FTIR spectra of BP-HCPs, (d) FTIR spectra of X-HCPs, (e) XPS survey spectra of BP-HCPs, and (f) XPS survey spectra of X-HCPs. FTIR spectral data between 1800 and 2800 cm^{-1} are omitted for clarity as no peaks were present in this region.

tical value (Table S1), likely due to the molecule's ability to effectively stabilise the carbocation formed upon the loss of Cl, aiding crosslink formation to the BCMBP monomer. However, the fluorine substituent is weakly deactivating toward electrophilic aromatic substitution and likely suppresses further propagation upon incorporation into the polymer. The presence of oxygen in all HCPs was ascribed to the attack of trace

water at the carbocation generated during the Friedel–Crafts reaction. In the fluorine-decorated HCPs, the high-resolution F 1s spectra displayed a peak at 687.5 eV, assigned to the C_{Ar}–F in the pFBC (Fig. S2). An additional peak at ~694 eV was observed, which does not correspond to known C–F species but is close to the binding energy of SF_6 (693.5 eV).[30] A plausible explanation for this feature may be residual sulfur con-

tamination, a common impurity in organic materials originating from crude oil cracking.

The high-resolution C 1s spectra of BP-HCPs and X-HCPs were deconvoluted into three peaks ~284.8 eV, 287.0 eV and 291.4 eV, corresponding to sp^2/sp^3 C, the combination of C–O and C–Cl, and a low-intensity $\pi \rightarrow \pi*$ shake-up feature,[30] respectively (Fig. S3). In fluorine-functionalised HCPs, C–F was expected to produce a peak at 286.0–286.5 eV but was not clearly distinguishable due to spectral overlap with C–O and C–Cl.

The TGA curves of all HCPs showed similar thermal stability (Fig. S4). All networks increased in weight at around 240 to 260 °C, indicative of oxidation,[15] before the onset of thermal decomposition at around 340 to 360 °C. All samples were decomposed completely at approximately 580 to 600 °C. The introduction of fluorine into the HCP networks did not noticeably alter their thermal stability.

N_2 adsorption–desorption isotherms of all samples were collected at −196 °C. According to IUPAC classification,[31] all networks displayed a combination of type I and type IV isotherms (Fig. 2a and b), consistent with typical HCPs.[14,32] The type I behaviour demonstrated by a steep uptake at low P/P_0 indicates microporosity, while the type IV component identified by hysteresis during desorption reflects mesoporous capillary condensation.

With increasing pFBC content, BP-HCPs exhibited a steady decline in porosity. The BET-specific surface areas (SSA_{BET}) decreased from 1748 ± 78 in BP-HCP to 960 ± 114 m^2 g^{-1} in BP-HCP-50F, with corresponding reductions in the total pore volume V_P, micropore volume V_{Mic}, and mesopore volume V_{Mes} (Table 2). On the other hand, porous properties remained relatively unchanged between X-HCP and X-HCP-25F, with SSA_{BET} of 1089 ± 105 m^2 g^{-1} and 1140 ± 94 m^2 g^{-1}, respectively, and an apparent increase in V_{Mes} from 0.61 cm^3 g^{-1} to 0.84 cm^3 g^{-1} was observed. However, at the highest pFBC loading (X-HCP-50F), porosity declined significantly, resulting in a SSA_{BET} of 691 ± 69 m^2 g^{-1} and V_{Mes} of 0.40 cm^3 g^{-1}. Overall, X-HCP networks derived a larger portion of their V_P from micropores than their BP-HCP counterparts (Table 2). Pore size distributions were determined using the QSDFT model, displaying an abundance of ~1 nm wide micropores and broad mesoporosity in all networks (Fig. 2c and d).
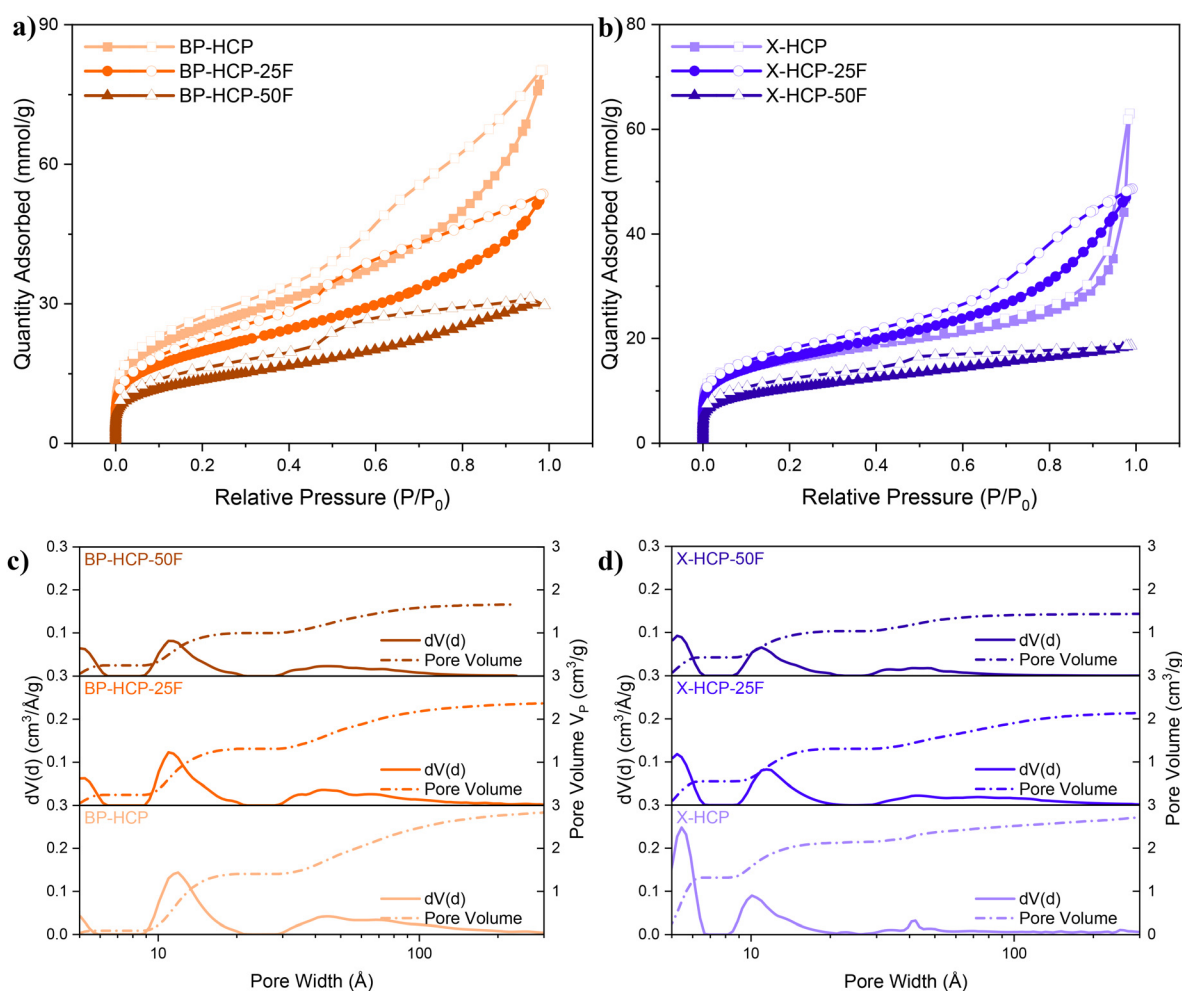

Fig. 2 (a) N$_2$ adsorption–desorption isotherms, and (c) pore size distribution and cumulative pore volume of BP-HCPs. (b) N$_2$ adsorption–desorption isotherms, and (d) pore size distribution and cumulative pore volume of X-HCPs.

© 2025 The Author(s). Published by the Royal Society of Chemistry

RSC Appl. Polym., 2025, **3**, 1315–1324 | **1319**

Table 2 Porous properties of all HCPs including BET-specific surface areas SSA$_{BET}$, total pore volumes V_P, micropore volume V_{Mic}, mesopore volume V_{Mes}, and ratio of V_{Mic} to V_{Mes}

Sample	SSA$_{BET}$ (m^2 g^{-1})	V_P (cm^3 g^{-1})	V_{Mic} (cm^3 g^{-1})	V_{Mes} (cm^3 g^{-1})	V_{Mic}/V_{Mes}
BP-HCP	1748 ± 78	2.85	1.40	1.45	1.0
BP-HCP-25F	1403 ± 182	2.38	1.31	1.07	1.2
BP-HCP-50F	960 ± 114	1.66	0.99	0.67	1.5
X-HCP	1089 ± 105	2.73	2.12	0.61	3.5
X-HCP-25F	1140 ± 94	2.14	1.30	0.84	1.6
X-HCP-50F	691 ± 69	1.43	1.03	0.40	2.6

Oil adsorption performance and oil/water separation performance of HCPs

To evaluate the adsorption performance of HCPs toward organic solvents, toluene, methanol, n-heptane, and DCE were selected as representative compounds of aromatic hydrocarbons, alcohols, linear alkanes, and halides, respectively. Adsorption experiments were conducted by suspending HCP samples in pure solvent and stirring for 1 h before removal of excess solvent by vacuum filtration. The HCPs were weighed immediately after filtration to minimise evaporation losses and then again after complete drying.

Adsorption capacity was calculated using two methods; the first, k_B, follows conventional literature approaches and considers the initial sample weight before adsorption. However, as the powdery HCPs in this work were recovered by vacuum filtration, some sample loss during filtration led to an underestimation of adsorption capacity. To correct for this loss, a second adsorption capacity, k_D, was calculated using the dry sample weight after adsorption, ensuring fairer comparison between networks. The k_D values were consistently only slightly higher than the corresponding k_B values (Table S2) and, therefore, remain comparable to k_B values in the literature. As such, k_D is used in the following discussion as a measure of adsorption capacity.

The adsorption capacities of the HCPs were compared with their SSA$_{BET}$ and V_P (Fig. 3 and Table S2). In the BP-HCP networks, adsorption capacities toward toluene and methanol decreased in line with SSA$_{BET}$ and V_P. Specifically, adsorption

dropped from 9.89 ± 0.49 to 3.55 ± 0.29 g g^{-1} for toluene and from 8.92 ± 1.52 to 3.99 ± 0.45 g g^{-1} for methanol, when comparing BP-HCP and B-HCP-50F. However, k_D did not follow the same trend for n-heptane and DCE; although both BP-HCP-25F and BP-HCP-50F exhibited lower adsorption than BP-HCP, a slight increase in uptake was observed in BP-HCP-50F. The higher fluorine content in BP-HCP-50F may enhance DCE adsorption via halogen interactions, while also improving n-heptane uptake due to its strong hydrophobicity. The hydrophobicity of BP-HCP-50F was assessed and compared to BP-HCP by the collection of dynamic vapour sorption isotherms of both toluene and water (Fig. S5). Although BP-HCP displayed a higher total uptake capacity for both water and toluene, the ratio of toluene : water total uptake was significantly larger in BP-HCP-50F (20 : 1) compared to BP-HCP (6 : 1), indicating increased hydrophobicity with the inclusion of fluorine.

Among the X-HCP polymers, the adsorption capacities for all four solvents again correlated closely to SSA$_{BET}$ and V_P (Table S2), remaining similar across X-HCP, X-HCP-25F, and decreasing for X-HCP-50F. In the X-HCPs, no positive effect on adsorption capacity was observed with the inclusion of fluorine. Overall, adsorption capacities correlated more closely with porosity rather than fluorine content, reinforcing the importance of pore structure in organic solvent uptake. The solvent adsorption capacity of our best performing material, BP-HCP, is compared with various oil adsorbents in the literature in Table S3.
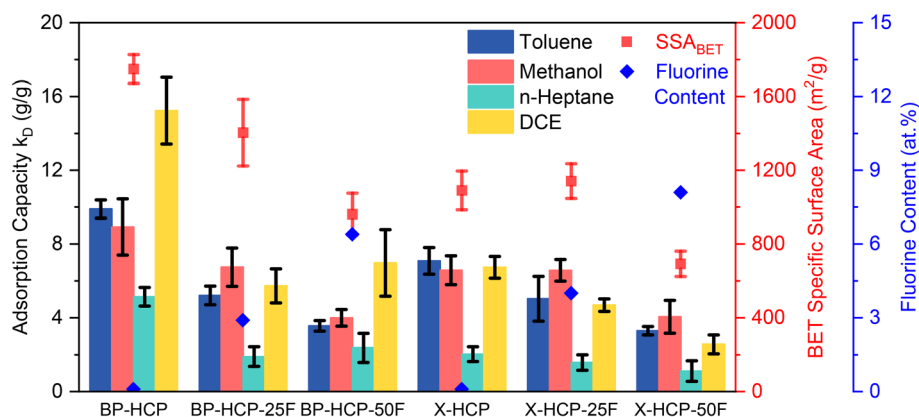
Fig. 3 Adsorption capacities k_D of HCPs for different organic solvents compared to their BET-specific surface area SSA$_{BET}$ and fluorine content.
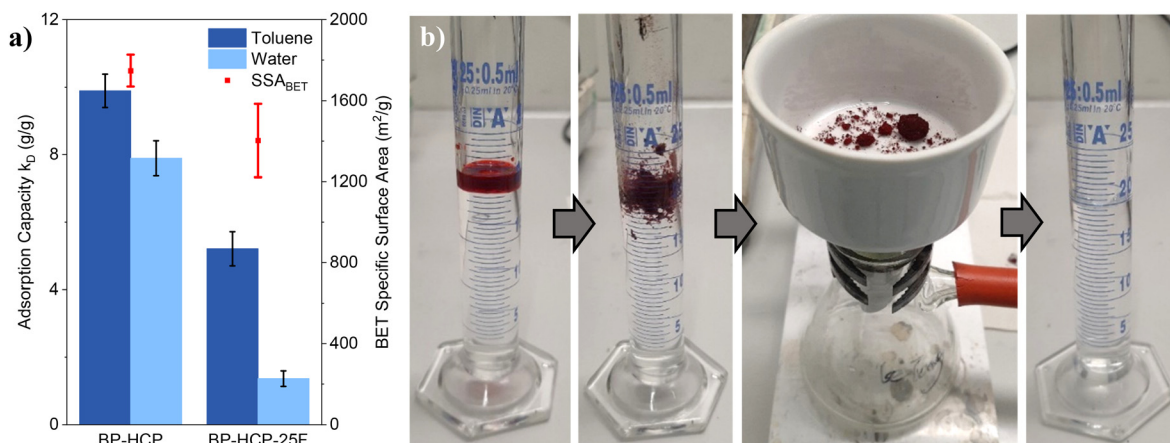
Fig. 4 (a) Adsorption capacities k_D of BP-HCP and BP-HCP-25F toward toluene and water, compared to their BET-specific surface areas. (b) Removal process of Sudan III dyed toluene from water using BP-HCP-25F.

The adsorption capacities k_D of BP-HCP and BP-HCP-25F toward distilled water were 7.89 ± 0.52 and 1.36 ± 0.23 g g^{-1}, respectively (Fig. 4a). The water adsorption performance of BP-HCP-25F was significantly lower than that of BP-HCP, caused by the combination of a reduction in SSA$_{BET}$ and V_P, as well as the hydrophobicity of the introduced p-fluorobenzyl groups, which may hinder water infiltration into the HCP pores.[24,26] Due to good apparent oil/water selectivity in isolated systems, BP-HCP and BP-HCP-25F were selected for testing in toluene/water separation experiments.

To visualise the oil/water separation process, Sudan III dye was added to toluene, and a model oil/water mixture was prepared by adding 0.5 mL of dyed toluene to 20 mL of distilled water. Both BP-HCP and BP-HCP-25F successfully adsorbed and removed the toluene from the water (Fig. 4b), demonstrating their applicability as adsorbents for oil/water separation. The adsorption efficiencies (AE) of BP-HCP and BP-HCP-25F reached up to 49.5% and 95.1%, respectively. The improved AE of BP-HCP-25F suggests that the increased hydrophobicity of the network improves efficiency in the toluene/water separation; however, this is more likely due to the addition of excess BP-HCP. It should be noted that this experiment was conducted as a proof of principle to observe oil/water separation

visually. We will seek to determine the limits of oil/water separation in future work.

The separation efficiencies (SE) of BP-HCP and BP-HCP-25F were determined by measuring the weight difference of the aqueous phase before and after separation, with both samples achieving 96% (Fig. S6). To account for potential water loss, a control experiment was conducted using water alone, allowing for the calculation of the actual separation efficiencies (SE$_a$) according to eqn (5):

$$SE_a = 100\% - SE_c + SE_m \quad (5)$$

where SE$_c$ represents the separation efficiency of the control and SE$_m$ the separation efficiency of the sample. After correcting for filtration-induced water loss, the SE$_a$ of BP-HCP and BP-HCP-25F were $99.5 \pm 0.4\%$ and $99.4 \pm 0.4\%$ (Fig. S6), respectively.

Despite the difference in oil/water selectivity between BP-HCP and BP-HCP-25F in isolated systems, the SE$_a$ was unchanged in the two-phase system, likely due to the general preference of both networks for the organic phase over water, as well as differences in experimental conditions compared with the ideal adsorption measurements.
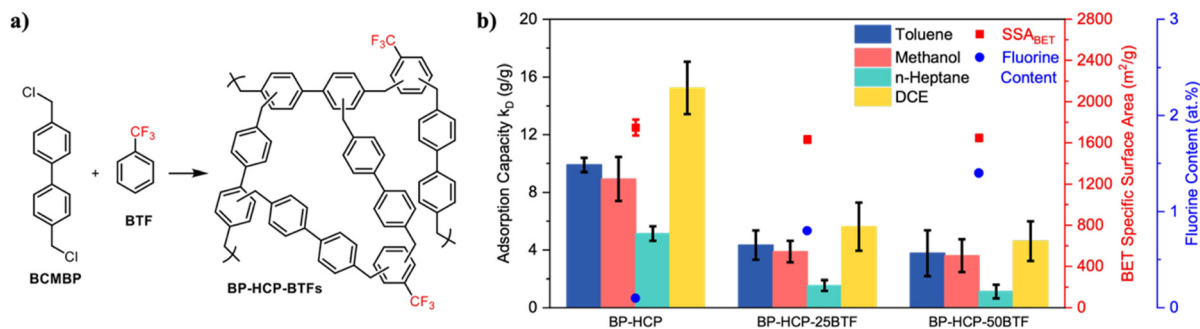

Fig. 5 (a) Reaction scheme for the synthesis of BP-HCPs. (b) Adsorption capacities k_D of BTF containing HCPs toward various organic solvents, their BET-specific surface areas SSA$_{BET}$, and fluorine contents.

© 2025 The Author(s). Published by the Royal Society of Chemistry

RSC Appl. Polym., 2025, **3**, 1315–1324 | **1321**

Recovery of HCP adsorbents

The HCPs exhibited excellent resistance to organic solvents and water, as confirmed by FTIR spectra and porous properties of the recovered samples (Fig. S7 and Table S4). Minimal changes in their chemical composition and SSA_{BET} after adsorption suggest that the structural integrity of HCPs remained intact, highlighting their suitability for the adsorption of oil from water and adsorbent recycling. Further details are shown and discussed in the SI.

To more thoroughly assess the impact of fluorine incorporation on oil adsorption in pure solvent systems, we also produced HCPs using trifluorotoluene (BTF) in place of pFBC in a BP-HCP series of networks (reaction scheme shown in Fig. 5a). A similar trend was observed in these networks to those discussed herein, with respect to their characterisation, adsorption of organics (Fig. 5b), and regeneration (complete data set shown in section 2 of the SI). In the BTF series, the strongly electron-withdrawing –CF$_3$ significantly reduces electrophilic reactivity, resulting in significantly reduced incorporation into the network compared to theoretical values (Table S5). Nevertheless, fluorine incorporation into HCPs again did not appear to benefit organic adsorption and, overall, BP-HCP remained the most promising candidate for oil/water separation.

Conclusions

In this study, a series of hypercrosslinked polymers were synthesised containing various concentrations of 4-fluorobenzyl chloride. The synthesis approach was facile and yielded networks with BET-specific surface areas up to 1750 m^2 g^{-1}, high thermal stability, and excellent resistance to organic solvents and water. Despite the controlled introduction of fluorine, the adsorption of pure organic solvents was primarily governed by porosity rather than chemical composition. Among the HCP networks, BP-HCP exhibited the highest porosity, with a surface area of 1750 m^2 g^{-1} and a total pore volume of 2.9 cm^3 g^{-1}, correlating well with its superior adsorption capacity for all solvents: 9.9 g g^{-1} for toluene, 8.9 g g^{-1} for methanol, 5.0 g g^{-1} for n-heptane, and 15.2 g g^{-1} for DCE. Furthermore, BP-HCP demonstrated excellent toluene/water separation with a separation efficiency of >99%. Our results confirm that fluorine incorporation did not enhance the network capacities for solvent adsorption, reinforcing that pore volume and surface area are most crucial for the adsorption process. These findings highlight BP-HCP's potential as a robust, reusable adsorbent for high-capacity oil/water separation, while also emphasising the importance of pore structure in the design of high-performance HCP-based oil/solvent adsorbents.

Conflicts of interest

There are no conflicts to declare.

Data availability

The data supporting this article have been included as part of the SI.

The SI includes additional experimental data, tables, and figures supporting the main text. It provides XPS-derived surface elemental compositions, FTIR spectra after long-term storage, and detailed XPS core-level spectra for all polymers. Additional TGA curves, N$_2$ adsorption–desorption isotherms, pore size distributions, and adsorption capacity data are presented, along with dynamic vapour sorption isotherms and oil/water separation efficiency measurements. Recovery studies are detailed through FTIR and porosity analyses of reused adsorbents. Comparative adsorption performance with literature materials is tabulated. Section 2 presents synthesis, characterisation, porosity, adsorption, and recovery data for trifluorotoluene-derived HCPs, BP-HCP-BTFs. See DOI: **https://doi.org/10.1039/d5lp00081e**.

Acknowledgements

References

1 A. Jernelöv, The threats from oil spills: now, then, and in the future, *Ambio*, 2010, **39**(5–6), 353–366, DOI: **10.1007/s13280-010-0085-5**.

2 N. Haridharan, D. Sundar, L. Kurrupasamy, A. Sambandam, C.-H. Liu and J. J. Wu, Oil spills adsorption and cleanup by polymeric materials: A review, *Polym. Adv. Technol.*, 2022, **33**(5), 1353–1384, DOI: **10.1002/pat.5636**.

3 J. Fu, J. Gong, Z. Zhao, S. E. O'Reilly and D. Zhao, Effects of Oil and Dispersant on Formation of Marine Oil Snow and Transport of Oil Hydrocarbons, *Environ. Sci. Technol.*, 2014, **48**(24), 14392–14399, DOI: **10.1021/es5042157**.

4 W. Zhang, N. Liu, L. Xu, R. Qu, Y. Chen, Q. Zhang, Y. Liu, Y. Wei and L. Feng, Polymer-Decorated Filter Material for Wastewater Treatment: In Situ Ultrafast Oil/Water Emulsion Separation and Azo Dye Adsorption, *Langmuir*, 2018, **34**, 13192–13202, DOI: **10.1021/acs.langmuir.8b02834**.

5 Q. Sheng, W. Tian and C. D. Wood, Hyper-cross-linked polymer-decorated surfaces with ultrahigh efficiency for oil/water emulsion separation and recovery, *ACS Appl. Mater. Interfaces*, 2021, **13**(33), 39925–39933, DOI: **10.1021/acsami.1c11302**.

6 C. Chen, D. Weng, A. Mahmood, S. Chen and J. Wang, Separation Mechanism and Construction of Surfaces with Special Wettability for Oil/Water Separation, *ACS Appl. Mater. Interfaces*, 2019, **11**(11), 11006–11027, DOI: **10.1021/acsami.9b01293**.

7 J. Huang, X. Ran, L. Sun, H. Bi and X. Wu, Recent advances in membrane technologies applied in oil–water separation, *Discover Nano*, 2024, **19**, 66, DOI: **10.1186/s11671-024-04012-w**.

8 B. Xiang, Q. Liu, Q. Sun, J. Gong, P. Mu and J. Li, Recent advances in eco-friendly fabrics with special wettability for oil/water separation, *Chem. Commun.*, 2022, **58**(97), 13413–13438, DOI: **10.1039/D2CC05780H**.

9 X. Li, M. Cao, H. Shan, F. H. Tezel and B. Li, Facile and scalable fabrication of superhydrophobic and superoleophilic PDMS-co-PMHS coating on porous substrates for highly effective oil/water separation, *Chem. Eng. J.*, 2019, **358**, 1101–1113, DOI: **10.1016/j.cej.2018.10.097**.

10 W. Zhang, N. Liu, Y. Cao, X. Lin, Y. Liu and L. Feng, Superwetting porous materials for wastewater treatment: from immiscible oil/water mixture to emulsion separation, *Adv. Mater. Interfaces*, 2017, **4**, 1600029, DOI: **10.1002/admi.201700029**.

11 J. Huang and S. R. Turner, Hypercrosslinked polymers: a review, *Polym. Rev.*, 2018, **58**(1), 1–41, DOI: **10.1080/15583724.2017.1344703**.

12 S. Raza, S. Nazeer, A. Abid and A. Kanwal, Recent research progress in the synthesis, characterization and applications of hyper cross-linked polymer, *J. Polym. Res.*, 2023, **30**(11), 415, DOI: **10.1007/s10965-023-03783-7**.

13 R. T. Woodward, L. A. Stevens, R. Dawson, M. Vijayaraghavan, T. Hasell, I. P. Silverwood, A. V. Ewing, T. Ratvijitvech, J. D. Exley, S. Y. Chong, F. Blanc, D. J. Adams, S. G. Kazarian, C. E. Snape, T. C. Drage and A. I. Cooper, Swellable, water- and acid-tolerant polymer sponges for chemoselective carbon dioxide capture, *J. Am. Chem. Soc.*, 2014, **136**(25), 9028–9035, DOI: **10.1021/ja5031968**.

14 P. Schweng, F. Mayer, D. Galehdari, K. Weiland and R. T. Woodward, A robust and low-cost sulfonated hyper-crosslinked polymer for atmospheric water harvesting, *Small*, 2023, **19**(50), e2304562, DOI: **10.1002/smll.202304562**.

15 P. Schweng, L. Präg and R. T. Woodward, Regulating the hydrophilicity of hyper-cross-linked polymers via thermal oxidation for atmospheric water harvesting, *ACS Appl. Mater. Interfaces*, 2024, **16**(43), 58566–58572, DOI: **10.1021/acsami.4c11013**.

16 W. Song, Y. Tang, B. Y. Moon, Q. Liao, H. Xu, Q. Hou, H. Zhang, D.-G. Yu, Y. Liao and I. Kim, Green synthesis of hypercrosslinked polymers for CO_2 capture and conversion: recent advances, opportunities, and challenges, *Green Chem.*, 2024, **26**(5), 2476–2504, DOI: **10.1039/D3GC04222G**.

17 G. Paul, F. Begni, A. Melicchio, G. Golemme, C. Bisio, D. Marchi, M. Cossi, L. Marchese and G. Gatti, Hyper-Cross-Linked Polymers for the Capture of Aromatic Volatile Compounds, *ACS Appl. Polym. Mater.*, 2020, **2**(2), 647–658, DOI: **10.1021/acsapm.9b01000**.

18 R. Castaldo, I. Berezovska, M. S. Silverstein and G. Gentile, PolyHIPEs Containing Hyper-Cross-Linked Resins: Hierarchical Porosity with Broad and Versatile Sorption

Properties, *ACS Appl. Polym. Mater.*, 2023, **5**(9), 6920–6931, DOI: **10.1021/acsapm.3c00974**.

19 F. Mayer, P. Schweng, S. Bräuer, S. Hummer, G. Koellensperger, A. Mautner, R. T. Woodward and A. Bismarck, Best of Both Worlds: Adsorptive ultrafiltration nanocellulose–hypercrosslinked polymer hybrid membranes for metal ion removal, *Small Sci.*, 2024, **4**(10), 2400182, DOI: **10.1002/smsc.202400182**.

20 J. Wolska, M. Frankowski, J. Jenczyk and L. Wolski, Highly sulfonated hyper-cross-linked polymers as promising adsorbents for efficient and selective removal of ciprofloxacin from water, *Sep. Purif. Technol.*, 2024, **343**, 127147, DOI: **10.1016/j.seppur.2024.127147**.

21 C. Karmelich, Z. Wan, W. Tian, E. Crooke, X. Qi, A. Carroll, K. Konstas and C. Wood, Advancing hyper-crosslinked materials with high efficiency and reusability for oil spill response, *Sci. Rep.*, 2023, **13**(1), 9779, DOI: **10.1038/s41598-023-36577-4**.

22 T. Xue, M. Wang, J. Man, Y. Yang, H. Miao and X. Li, Construction and Regulation of a Superhydrophobic Sponge via In Situ Anchoring of a Hyper-Cross-Linked Polymer for Efficient Oil/Water Separation, *ACS Appl. Polym. Mater.*, 2024, **6**(7), 3864–3874, DOI: **10.1021/acsapm.3c03130**.

23 J. Lin, X. Xia, Y. Liu, Z. Luan, Y. Chen, K. Ma, B. Geng and H. Li, Fabrication of hierarchical porous fluoro–PolyHIPE materials with ultra–high specific surface area via hyper-crosslinking knitting technique, *J. Appl. Polym. Sci.*, 2022, **139**(38), e52914, DOI: **10.1002/app.52914**.

24 N. Zhang, Y. Qi, Y. Zhang, J. Luo, P. Cui and W. Jiang, A review on oil/water mixture separation material, *Ind. Eng. Chem. Res.*, 2020, **59**(33), 14546–14568, DOI: **10.1021/acs.iecr.0c02524**.

25 S. Ruidas, A. Das, S. Kumar, S. Dalapati, U. Manna and A. Bhaumik, Non-fluorinated and robust superhydrophobic modification on covalent organic frameworks for crude-oil-in-water emulsion separation, *Angew. Chem., Int. Ed.*, 2022, **61**(41), e202210507, DOI: **10.1002/ange.202210507**.

26 C. M. Navarathna, N. Bombuwala Dewage, C. Keeton, J. Pennisson, R. Henderson, B. Lashley, X. Zhang, E. B. Hassan, F. Perez and D. Mohan, Biochar adsorbents with enhanced hydrophobicity for oil spill removal, *ACS Appl. Mater. Interfaces*, 2020, **12**(8), 9248–9260, DOI: **10.1021/acsami.9b20924**.

27 L. Yang, Z. Wang, L. Yang, X. Li, Y. Zhang and C. Lu, Coco peat powder as a source of magnetic sorbent for selective oil–water separation, *Ind. Crops Prod.*, 2017, **101**, 1–10, DOI: **10.1016/j.indcrop.2017.02.040**.

28 C. D. Wood, B. Tan, A. Trewin, H. Niu, D. Bradshaw, M. J. Rosseinsky, Y. Z. Khimyak, N. L. Campbell, R. Kirk, E. Stöckel and A. I. Cooper, Hydrogen storage in microporous hypercrosslinked organic polymer networks, *Chem. Mater.*, 2007, **19**(8), 2034–2048, DOI: **10.1021/cm070356a**.

29 A. Sarkar and S. Mahapatra, Novel hydrophobic vaterite particles for oil removal and recovery, *J. Mater. Chem. A*, 2014, **2**(11), 3808–3818, DOI: **10.1039/C3TA14450J**.

© 2025 The Author(s). Published by the Royal Society of Chemistry

RSC Appl. Polym., 2025, **3**, 1315–1324 | **1323**

30 B. Vincent, The International XPS Database, 2021–2024 [accessed June 9, 2025]; available from: **https://xpsdatabase. net/**.

31 M. Thommes, K. Kaneko, A. V. Neimark, J. P. Olivier, F. Rodriguez-Reinoso, J. Rouquerol and K. S. Sing, Physisorption of gases, with special reference to the evaluation of surface area and pore size distribution (IUPAC Technical Report), *Pure Appl. Chem.*, 2015, **87**(9–10), 1051–1069, DOI: **10.1515/pac-2014-1117**.

32 L. Prince, P. Guggenberger, E. Santini, F. Kleitz and R. T. Woodward, Metal-Free Hyper-Cross-Linked Polymers from Benzyl Methyl Ethers: A Route to Polymerization Catalyst Recycling, *Macromolecules*, 2021, **54**(19), 9217–9222, DOI: **10.1021/acs.macromol.1c01332**.